

VARGAN: Variance Enforcing Network Enhanced GAN

Sanaz Mohammadjafari · Mucahit Cevik ·
Ayse Basar

Received: date / Accepted: date

Abstract Generative adversarial networks (GANs) are one of the most widely used generative models. GANs can learn complex multi-modal distributions, and generate real-like samples. Despite the major success of GANs in generating synthetic data, they might suffer from unstable training process, and mode collapse. In this paper, we introduce a new GAN architecture called variance enforcing GAN (VARGAN), which incorporates a third network to introduce diversity in the generated samples. The third network measures the diversity of the generated samples, which is used to penalize the generator's loss for low diversity samples. The network is trained on the available training data and undesired distributions with limited modality. On a set of synthetic and real-world image data, VARGAN generates a more diverse set of samples compared to the recent state-of-the-art models. High diversity and low computational complexity, as well as fast convergence, make VARGAN a promising model to alleviate mode collapse.

Keywords Generative adversarial networks, mode collapse, multi-modal distribution, variance enforcing network

1 Introduction

Generative Adversarial Networks (GANs) have emerged as a powerful generative model at learning data distributions. GANs have displayed a great potential in generating high quality images (Karras et al., 2017; Brock et al., 2018), and have been successfully used for image super-resolution (Bin et al., 2017; Ledig et al., 2017) and image-to-image translation (Isola et al., 2017; Zhu et al., 2017a). GANs

Sanaz Mohammadjafari
Data Science Lab, Ryerson University, Toronto, Canada
E-mail: sanaz.mohammadjafari@ryerson.ca

Mucahit Cevik
Data Science Lab, Ryerson University, Toronto, Canada

Ayse Basar
Data Science Lab, Ryerson University, Toronto, Canada

consist of a generator network responsible for generating samples similar to the true distribution, and a discriminator network that discriminates between the samples from the true and generated distributions. GANs aim to generate a set of samples that represent the true distribution, preserve the image quality and cover all the modes. Achieving these goals rely on several factors such as model structure, network’s objective functions, parameter tuning and training procedure. Although GANs have shown great potential in generating synthetic data, their unstable training procedure can cause non-convergence, and mode collapse (Salimans et al., 2016).

Mode collapse refers to generating a limited number of modes from a multi-modal training data, and failing to generate a representative set of samples. This problem has limited GANs’ potential in real-world applications such as MRI scan generation for brain segmentation (Mok and Chung, 2018) and electromagnetic engineered surface (EES) generation to improve the radio signal coverage in telecommunication (Mohammadjafari et al., 2021). A large and growing body of literature has investigated various methods to alleviate the mode collapse issue in GANs through modified loss functions (Arjovsky et al., 2017; Che et al., 2016; Gulrajani et al., 2017), altering neural network structures (Zuo et al., 2019; Lin et al., 2018), adapting different training methods (Metz et al., 2016) and latent space regularization (Gurumurthy et al., 2017; Li et al., 2021). Regardless of the methodological differences, the proposed studies fall short of identifying a global solution.

In this work, we focus on the problem of mode collapse in GANs for image generation. Particularly, we are interested in binary and gray-scale images because of GANs’ practical applications. For instance, effective usage of GANs in generating binary EES designs has been established in (Mohammadjafari et al., 2021). However, cases of mode collapse were observed in the results, which affected the sample generation process. Moreover, research on image generation has been mostly restricted to colored image datasets. Therefore, our research can offer particular insights into binary and gray-scale image generation. Furthermore, binary and gray-scale image generation process requires a less complex model structure, and as a result, has lower computational complexity compared to the colored images. On the other hand, there could be certain challenges with binary images. For instance, category of binary EES designs changes rapidly by small changes in the image, which makes the training process of GANs for these binary images more challenging, requiring more research in this direction.

Research goal In this paper, we propose a novel GAN architecture called variance enforcing GAN (VARGAN) to alleviate the mode collapse problem in image generation, and increase the diversity of generated samples. We evaluate our method on two widely used datasets in the literature namely, 2D synthetic data and stacked MNIST, as well as on the real-life practical problem of generating EES designs. Furthermore, considering the practical importance of conditional GANs, we examine the impact of conditioning on the mode collapse.

Contributions The main contribution of our paper is proposing a novel GAN architecture called VARGAN, which uses a third network called variance enforcing network (VarNet) to increase the number of generated modes, and reduce the mode collapse. Major contributions of our study can be summarized as follows:

- Our proposed method introduces a third network trained to compute the generated samples’ diversity. VARGAN shows performance improvement over state-of-the-art GAN models in the literature.
- We explore the impact of conditioning and labels’ length on mode collapse. We hypothesize that conditioning the GANs on auxiliary information can majorly impact the number of uniquely generated modes. The results show how VARGAN’s performance, unlike other models, is not impacted by the length of conditioning labels.
- We perform an extensive numerical study to evaluate GAN variants’ performance on addressing the mode collapse using a variety of synthetic and real datasets. The results are analyzed based on various performance metrics employed in recent studies. Specifically, we provide a detailed comparative analysis for different GAN architectures on a practical problem, EES generation, which has a significant application in telecommunication industry. Alleviating mode collapse problem and increasing the generated unique designs can greatly contribute to EES generation process by identifying designs that are not otherwise easy to obtain.

Organization of the paper: The rest of this paper is organized as follows. Section 2 summarizes the recent work on methods to address the mode collapse issue in GANs. In Section 3, generic GAN structures are presented, and the methodology of the proposed architecture, as well as its training process are explained. Section 3 also covers the comparison of proposed method with the state-of-the-art GAN models. Section 4 provides a discussion on the model performance for different types of datasets. Finally, the paper is concluded in Section 5, and possible future directions are discussed.

2 Background

In this section, we review recent studies on GANs with a special focus on mode collapse issue. A summary of the recent papers is reported in Table 1, which contains information on the methodology, GAN structures and datasets used in the numerical experiments.

Salimans et al. (2016) proposed several approaches based on modifications in GANs’ architecture and loss functions. Feature matching, historical averaging and mini-batch discrimination are examples of the methods proposed to improve the convergence and mode collapse in GANs. Mini-batch discrimination approach adds a new component to the last layer of discriminator by computing the distance among the last layer’s samples. The authors claim that closer samples are more likely to be created by the generator, and their proposed enhancements help with discriminator’s decision making and improves GAN’s convergence.

Table 1: Summary of the relevant papers addressing the mode collapse (FF: Feed-forward, ConvGAN: Convolutional GAN, cCGAN: Conditional Convolutional GAN).

Paper	Proposed method	Methodology	GAN structure	Dataset
Salimans et al. (2016)	Minibatch discrimination	Distance of extracted features in the last layer of discriminator added to discriminator's loss as penalty	ConvGAN	MNIST [†] CIFAR-10
Che et al. (2016)	Mode regularized GAN	Jointly train an encoder add penalty factors to generator's loss function	ConvGAN	Stacked MNIST CelebA
Arjovsky et al. (2017)	Wasserstein GAN	Wasserstein distance plus weight clipping	ConvGAN	LSUN-Bedrooms
Gulrajani et al. (2017)	WGAN-GP	Replace weight clipping in Wasserstein GANs with an enforced Lipschitz constraint	ConvGAN	LSUN-Bedrooms CIFAR-10
Tolstikhin et al. (2017)	AdaGAN	Mixture of GANs trained on reweighted samples	ConvGAN FF GAN	MNIST [†] Stacked MNIST Synthetic data [†]
Park et al. (2018)	MEGAN	Mixture of GANs	ConvGAN	CelebA LSUN-Church outdoor
Lin et al. (2018)	PacGAN	Discriminator's architecture receives m samples at a time	ConvGAN FF GAN	Stacked MNIST CelebA Synthetic data [†]
Ghosh et al. (2018)	MADGAN	Multi-generators	FF GAN ConvGAN cCGAN	Synthetic data Stacked MNIST CelebA Night-to-day Edges-to-handbags
Elfeki et al. (2019)	GDPP	Use negative correlations within a subset as diversity measure added to generator's loss	FF GAN ConvGAN	Synthetic data Stacked MNIST CIFAR-10
Mao et al. (2019)	MSGAN	Image difference divided by noise difference added to generator's loss function	Conditioned on labels Conditioned on Images Text to image synthesis	CIFAR-10 Winter-to-summer CUB-200-2011
Our study	VARGAN	A third network trained on samples' diversity adds a penalty to the generator's loss to encourage diversity	FF GAN FF GAN, ConvGAN	Synthetic data [†] Stacked MNIST EES* [†]

* propriety dataset

[†] gray scale images

Altering the loss function to stabilize GANs' training, and to increase the covered modes is investigated in various studies. These methods include introducing new distance metrics such as Wasserstein distance (Arjovsky et al., 2017), incorporating regularization penalties for cost functions of the networks (Che et al., 2016; Gulrajani et al., 2017), and encouraging diversity in generated samples through an unsupervised penalty loss based on the samples in last layer of the discriminator (Elfeki et al., 2019). Previous studies often evaluated the impact of modifications in neural networks' structures by changing GANs' networks architectures, and incorporation of multiple networks to cover the missed modes (Park et al., 2018; Hoang et al., 2018; Srivastava et al., 2017; Zhong et al., 2019). For instance, Lin et al. (2018) altered the discriminator's architecture to receive m merged samples of the data with the same label (fake or real) and generate one label instead of m . Their proposed method, PacGAN, showed great improvement in fake samples' diversity. GANs construction using multiple networks is inspired by the theory established for mode collapse in (Arjovsky and Bottou, 2017) where disjoint distribution of real and generated data is considered as the source of instability and missed modes. Multi-agent GAN (MADGAN) is one particular approach that contains multiple generators and one discriminator network to encourage different generators toward separate modes of the data, and increase the variety of generated samples (Ghosh et al., 2018). Tolstikhin et al. (2017) proposed adaptive GAN (AdaGAN), which incrementally adds a new model to a mixture of GANs, and evaluates a new GAN model on re-weighted samples.

Majority of the studies investigating mode collapse consider vanilla GANs structures and exclude conditional GANs as shown in Table 1. However, conditional GAN architectures have a wide range of applications in many areas (Isola et al., 2017; Zhu et al., 2017a; Mohammadjafari et al., 2021). They also suffer from mode collapse, which has been investigated in a limited number of studies. Zhu et al. (2017b) proposed a new hybrid GAN structure namely, Bicycle GAN, which incorporates bidirectional mapping from latent code to output. This study was implemented on particular conditional tasks, and has a significant computational complexity overhead. Mao et al. (2019) proposed a new general approach called MSGAN by adding a regularization term to the generator's loss function that is applicable to various GAN architectures. MSGAN approach encourages the generator to map two different samples conditioned on the same context to be as distant from each other as possible.

Our VARGAN method utilizes some of the aforementioned enhancements such as modified loss functions and adding a new penalty term to the generator's loss (e.g., see (Elfeki et al., 2019)), which computes the generated samples' diversity. However, in contrast to the previous approaches, our proposed penalty term is calculated by a third network trained on various sets of training samples with their relative diversity level. Different than multi-network approaches, our method does not incorporate a new generator or a discriminator, and the third network is solely responsible to provide feedback to the generator. Moreover, our approach incorporates the same strategy of modified structures as (Lin et al., 2018) for its new network's architecture.

3 Methodology

In this section, we describe our methods, datasets and the experimental setup. We first review the structure of the vanilla GAN and its training procedure, and then explain the VARGAN architecture in detail. In addition, we discuss how our proposed framework compares to the existing GAN architectures.

3.1 Standard GAN models

A generic GAN architecture consists of two networks known as the generator and the discriminator, both competing against each other (see Figure 1). The generator learns the distribution p_g from a uniform or normal distribution input noise z mapped through the function $G(z; \theta_g)$ to the samples. $G(z; \theta_g)$ is a differentiable function, usually defined as a neural network with a set of parameters θ_g . The discriminator $D(x, \theta_d)$, which is also a differentiable function with parameters θ_d , maps input samples to a probability value representing whether each sample is real or generated. Both networks are trained simultaneously, where discriminator aims to maximize and generator tries to minimize the objective value. Therefore, GAN is modelled as a min-max game with a value function $V(D, G)$, that is

$$\min_G \max_D V(D, G) = E_{x \sim p_{data}(x)} [\log D(x)] + E_{z \sim p_z(z)} [\log(1 - D(G(z)))] \quad (1)$$

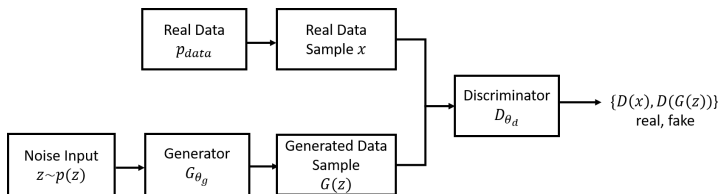


Fig. 1: GAN structure consists of two competing networks, namely, discriminator and generator

The discriminator aims to maximize the value function by generating a probability value of one for the samples from the real data p_{data} and zero for the samples from the generated distribution p_g . On the other hand, generator minimizes the objective value by trying to trick the discriminator into outputting one for the generated samples. The training procedure of the GANs' networks is illustrated in Figure 2.

Vanilla GAN has no control on the category of the generated samples. Therefore, conditional GANs were proposed to incorporate supplemental data as labels in both the generator and discriminator, and generate samples of a desirable category (Mirza and Osindero, 2014). Convolutional GANs are another important variant of GANs that use convolutional neural network (CNN) instead of feed-forward structure in their networks (Radford et al., 2015).

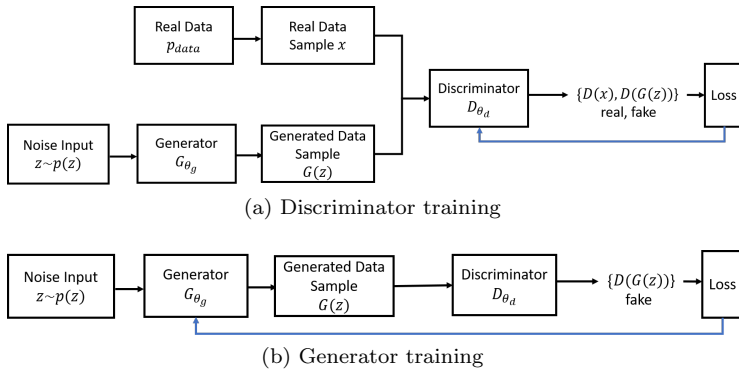


Fig. 2: GAN model training procedure including discriminator and generator feedback signals

3.2 VARGAN

We propose a new GAN framework called VARGAN illustrated in Figure 3 by introducing a third network called VarNet to the vanilla GAN structure. The VarNet is used to reduce the mode collapse by encouraging diversity in the generated samples, which results in increased number of generated modes. Below, we describe VARGAN architecture and the training procedure.

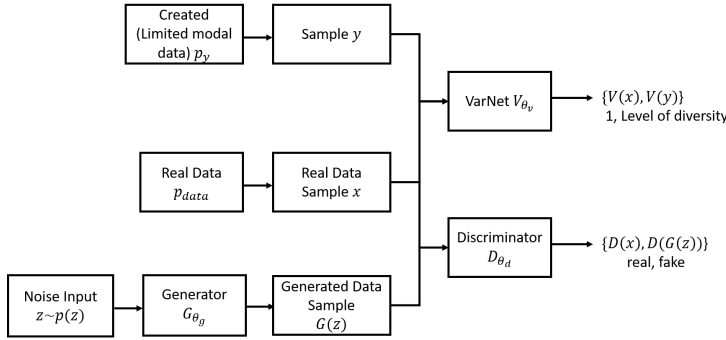


Fig. 3: VARGAN structure including generator, discriminator and VarNet networks

3.2.1 Data samples

Discriminator network in GANs utilizes two sets of data for its training process, namely, the real and fake data. GAN aims to learn the real data distribution p_{data} with N number of unique modes. Therefore, N is the target and highest number of unique modes in p_{data} that a generator can create. It is important to note that for some datasets with unknown number of unique modes, we can select different

N values to encourage the diversity. Fake data distribution p_g is created by the generator network that needs to improve in quality and diversity to reach the true distribution.

In the VARGAN framework, we introduce another set of data called limited modality data p_y , which defines the undesirable distributions with restricted number of modes. The limited modality data is used for VarNet training process. The undesirable distributions include lower number of modes than the target data with different sample distributions. Different than real and fake data, limited modality data is created by following a specific set of rules and using the real data.

The first step in creating p_y is to define the number of modes $n < N$ that data sample covers, which is less than the target number of modes. Then, we select n different data points from the batch of training data and repeat each of them $\frac{B}{n}$ times to create a uniform set of n different categories in the batch, where B represents the batch size. Each created batch of data with n different modes has a relative Mode Coverage Ratio (MCR) value between zero and one, which is defined as follows:

$$\text{MCR} = \begin{cases} \frac{L}{1 + S_1 \cdot e^{-\frac{n}{N} \cdot S_2}} & n = 2, \dots, N-1, L \in (0, 1], n \mid B \\ 0 & n = 1 \end{cases} \quad (2)$$

MCR value of zero indicates a single unique design in the sample, representing the lowest level of diversity. As the number of modes increase, the MCR value increases as well. Equation (2) shows the MCR value as a function of the modes (n) divided by the target number of modes (N), representing the percentage of generated modes. Parameters L , S_1 and S_2 are the constants that control the MCR trajectory. Comparison of Figure 4b and 4a shows how L controls the final value of MCR for high number of modes by using two different values for L . Figure 4 also illustrates how S_1 controls the initial value of MCR. A small MCR value for low number of covered modes can increase the generator’s loss at the beginning steps of the training process. This can adversely affect the model convergence, and needs to be controlled. Moreover, a high MCR value for low number of modes can prevent the generator from further increasing the diversity. Parameter S_2 controls the slope of the MCR, and since slope affects the model’s convergence process, S_2 affects the convergence to the target MCR value. These constants are determined through preliminary analysis (see details in Appendix A). Generation of limited modality data and the relative MCR remains a challenging part of the VARGAN framework, since it enforces a few constraints on the number of selected modes. One constraint is that the number of modes should divide the batch size because of the VarNet structure explained in the following sections.

3.2.2 VARGAN architecture

The VARGAN framework maintains the same discriminator and generator architecture as the standard GANs. The new network, VarNet $V(x, \theta_v)$ is a differentiable function created by a neural network with θ_v parameters that associates each set of input samples to an MCR value. As shown in Figure 3, the VarNet receives a sample data x from real data distribution p_{data} , and a sample data y from limited modality data p_y , and maps them to a single scalar value between zero and one representing the level of diversity of the samples. The VarNet network employs the

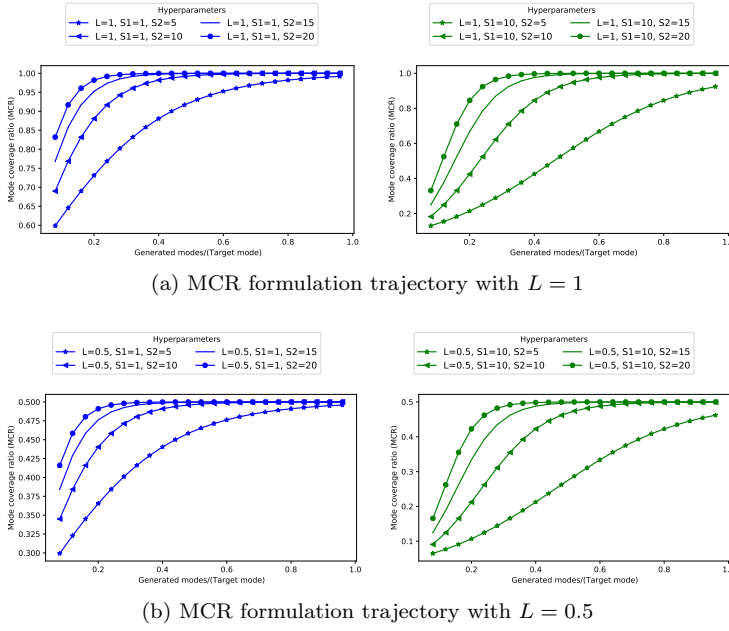


Fig. 4: MCR formulation trajectory with respect to the number of generated modes divided by the target number of modes using different hyperparameter values for L , S_1 and S_2

PacGAN structure (Lin et al., 2018) with a degree of packing equal to the batch size. The packing degree m refers to the number of augmented samples with the same label. In our case, packing degree is equal to the batch number indicating that VarNet receives the whole batch of the data $V(X_1, X_2, \dots, X_m)$ and maps it to one MCR value. Note that since packing number m is equal to B , n needs to divide batch size B to have a reasonable MCR value for each batch. A sample of limited data set with $n = 3$ and batch size of six passed to a VarNet is illustrated in Figure 5.

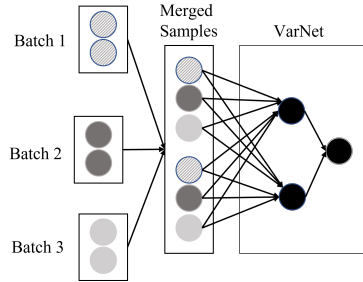


Fig. 5: Limited modality data with $n = 3$ and $B = 6$ passed to a sample VarNet structure with $m = 6$ with one output

3.2.3 VARGAN training process

The VARGAN training procedure is presented in Figure 6. The loss function for VarNet training is as follows:

$$\min_V F(V) = E_{x \sim p_{data}(x)}[\log(1 - V(x))] + E_{y \sim p_y(y)}[\log(MCR - V(y))] \quad (3)$$

The network receives two sets of inputs for the training process. The first one is a sample of training data $p(x)$ with the target distribution and a high MCR value as labels. The second input is a set of limited modality data $p(y)$ with different MCR values. The VarNet aims to minimize loss value by mapping the training data samples to label one and the limited modality data to the relative MCR. The structure and loss function of the discriminator for VARGAN remain the same compared to generic GAN architecture (see Figure 2a). However, the generator's loss function has a new addition provided in Equation (4) as follows:

$$\begin{aligned} \min_G F(D, G, V) = & E_{z \sim p_z(z)}[\log(1 - D(G(z)))] \\ & + E_{z \sim p_z(z)}[\log(1 - V(G(z)))] \cdot C \end{aligned} \quad (4)$$

The new term calculates the loss between the target level of MCR, which is one, and the MCR of the generator's outputs measured by VarNet. This term is also multiplied with a positive coefficient factor $C \leq 1$, which controls the impact of VarNet on generator's loss. The value of parameter C is selected based on hyperparameter tuning experiments and for the majority of the experiments, it is found to be one.

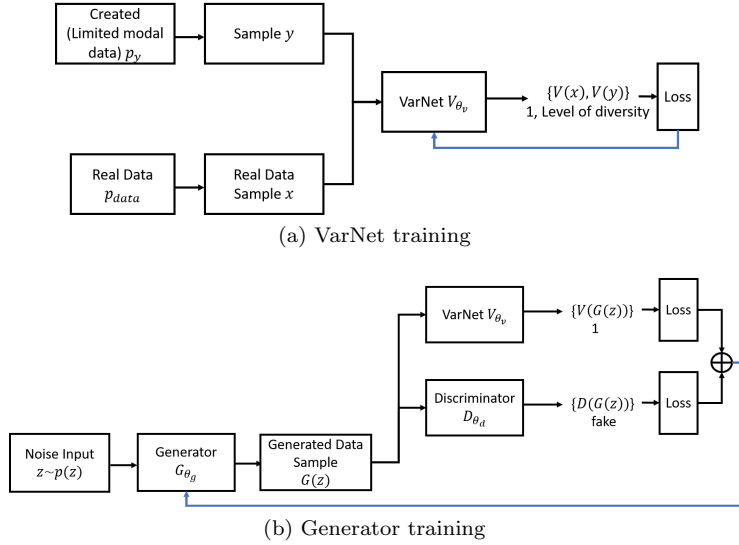


Fig. 6: Training procedures VARGAN networks including VarNet and generator (discriminator's training process is similar to vanilla GAN and is not illustrated).

3.2.4 Comparison with other architectures

VARGAN employs similar strategies to other available GAN architectures to deal with mode collapse issue. Our proposed framework incorporates the generated samples diversity in each iteration to penalize the generator towards a multi-modal output. The idea of penalizing the generator for the diversity is also discussed in (Elfeki et al., 2019) where Determinantal Point Process (DPP) is used to compute the diversity from the features of the discriminator’s last layer. However, in our work, a third network is trained to evaluate the samples diversity. Also note that our approach differs from multi-network models. VARGAN does not rely on any additional generator or discriminator networks. The third network (VarNet) sends an additional feedback to the generator to help with the diversity. We incorporate the same methodology of modified structures as (Lin et al., 2018) for the VarNet architecture to help the model differentiate between samples. However, the main contribution of our model to address the mode collapse issue is the additional penalty term added to the generator. Moreover, mini-batch discrimination (Salimans et al., 2016) incorporates a distance measure in the discriminator architecture to help distinguish between real and fake samples, which is not employed in our VARGAN architecture.

3.3 Datasets

We consider three particular datasets in our numerical study, which are described below.

- *Synthetic data*: We experiment with a number of synthetic datasets that have been considered in previous studies. The 2D ring dataset is a mixture of eight 2D Gaussians with mean $(\cos((2\pi/8)i), \sin((2\pi/8)i))$, and standard deviation of 0.01 in each dimension for $i \in \{1, \dots, 8\}$. We also experiment with a 2D grid dataset, which is a mixture of 25 and 36, 2D Gaussians with mean $(-1 + 0.4i, -1 + 0.4j)$ and standard deviation of 0.05 in each dimension for $i, j \in \{0, 1, \dots, n\}$ where n is the root square of number of mixture modes. Examples of synthetic data are illustrated in Figure 7.

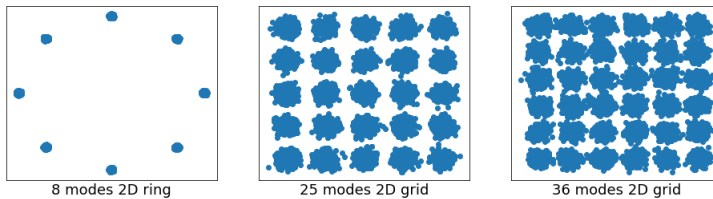


Fig. 7: Synthetic data

- *Stacked MNIST*: Stacked MNIST data contains three channels, each presenting one digit from the MNIST dataset. Therefore, the stacked MNIST dataset covers 1000 different modes illustrated in Figure 8.

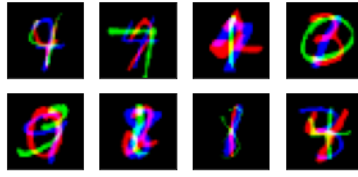


Fig. 8: Stacked MNIST data

- *EES dataset*: Original EES dataset consists of full-wave electromagnetic simulations with the element shape represented by a binary image and its corresponding transmission response over frequency. The EES element shapes are 2D binary images with 8-fold-symmetry where a single octant of the image contains sufficient information to fully describe the topology. The exhaustive search space includes 32,768 unique designs, which are all the possible combinations of the binary 15 bits, representing $\frac{1}{8}$ of the image. Similar dataset is generated for 19×19 designs, though unlike the 9×9 design dataset, it only contains a small subset of the corresponding search space.

A sample set of EES elements is shown in Figure 9. The high pass (HP) and low pass (LP) designs are the two main categories of EES designs. In the EES dataset, the high pass designs, unlike low pass designs, have edge to edge connection, which is illustrated in Figure 9a. As mentioned above, the whole search space is available for 9×9 designs; however, for 19×19 designs, 100,000 samples form the respective dataset. The dataset used in this paper is synthetically generated based on the structural configurations of the original dataset considered in (Mohammadjafari et al., 2021).



Fig. 9: EES dataset

3.4 Experimental setup

We evaluate our proposed VARGAN architecture on three different datasets and compare the performance with vanilla GAN and other popular GAN variants from the literature. Models include GANs with mini-batch discrimination (MB) (Salimans et al., 2016), PacGAN (Lin et al., 2018) with packing factor of four, MADGAN (Ghosh et al., 2018) with four generators, GDPP (Elfeki et al., 2019) and PacVARGAN. PacVARGAN is a new model with a discriminator network

incorporating the PacGAN structure with a packing factor of four and an additional VarNet network. Although, GAN structures in our experiments are not conditional, in the second part of our experiments, we investigate the effect of conditioning on the mode collapse. We add the categories as labels to the best performing unconditioned model and compare the performance with baseline vanilla GAN models. Only EES dataset is used for conditional GAN experiments.

The feed-forward (FF) GAN architecture is similar for all the datasets, whereas the convolutional GAN structure is dataset dependent, and reported in Appendix B for stacked MNIST and EES datasets. For the synthetic 2D data, a feed-forward architecture is selected, since data does not benefit from a convolutional structure. On the other hand, for stacked MNIST and EES, both feed-forward and convolutional neural networks are employed.

For synthetic and stacked MNIST data, each model is trained on 100,000 training samples and tested on 26,000 samples. For all the networks, Adam optimizer with a learning rate of $2e - 4$ is used. For the EES data, each model is trained on 100,000 samples for 19×19 designs, and on all the designs in the search space for 9×9 designs. The models are evaluated on 20,000 samples per category. The model is trained for 50, 30 and 400 epochs for synthetic, stacked MNIST and EES data. In VARGAN, MCR parameter values, namely, L , S_1 , S_2 , and C are selected as 1, 10, 5, and 1 across all datasets based on our hyperparameter tuning experiments (see Appendix A). In our numerical study, to minimize the random initialization effect, each experiment is repeated five times and average performance values are reported. All the models were implemented using Python and PyTorch library, and experiments were performed on a NVIDIA GeForce RTX 2070 GPU with 8 GB of GPU RAM.

4 Numerical results

In this section, we first present performance metrics used to evaluate GAN architectures. Then, we report the performance of GAN architectures over a variety of datasets. Finally, we investigate the impact of conditioning on mode collapse in GANs.

4.1 Performance metrics

Evaluating mode collapse is a challenging task, except in cases such as synthetic data where the modes are explicitly defined. Therefore, in this work, each GAN architecture is evaluated based on a set of popular performance metrics relevant to the dataset specifications. Since the labels are available for each dataset, a pre-trained classifier is used to determine the *number of modes* generated by the models. The *number of modes* and *Kullback-Leibler (KL) divergence*, which measures the distance between the generated and real distributions are reported for each model over all the datasets. *Percentage of high-quality samples* is another metric introduced in (Lin et al., 2018) for evaluating model performance over a synthetic dataset. It measures the proportion of generated samples that are closer than 3 standard deviations to the center of the mode. Finally, for the stacked MNIST data, we use the *inception score* to evaluate the quality and diversity of the generated samples

(Salimans et al., 2016). It is important to note that the run time performance in each experiment is reported based on the model’s training time in seconds, and does not reflect the theoretical complexity.

4.2 Comparison of GAN architectures

In this section, we report performance evaluation results for different GAN architectures over synthetic and real-world datasets. Along with our extensive comparative analysis, we also investigate the convergence behaviours of the models over training epochs in the training process.

4.2.1 Results with synthetic dataset

We have reported the number of generated modes, KL divergence and percentage of high-quality samples for each synthetic dataset variants separately. As shown in Table 2, for 2D grids with 25 and 36 modes, VARGAN captures all the modes with low divergence metric while generating high quality samples, and requiring less training time.

We note that VARGAN does not perform well for 2D ring with 8 modes, whereas PacGAN generates a high number of modes as well as high quality samples. Overall, it is observed that PacGAN consistently generates more unique samples with better quality for all three groups of synthetic data. However, the training times for PacGAN is much higher than other models, and is almost equal to the vanilla GAN model. Our results for PacGAN model on 2D ring and 2D grid with 25 modes are consistent with the findings in (Lin et al., 2018). By combining the PacGAN properties with VARGAN, PacVARGAN shows both high number of generated modes and low run times. We also find that mini-batch discrimination does not perform well for different designs. The reason can be the network’s feed-forward architecture that cannot benefit from mini-batch discrimination approach in addressing the mode collapse. MADGAN outperforms mini-batch discrimination, but still does not perform as well as other models. Moreover, GDPP generates high number of unique designs that match the findings of Elfeki et al. (2019). We find that VARGAN outperforms GDPP in terms of percentage of high quality samples and KL divergence.

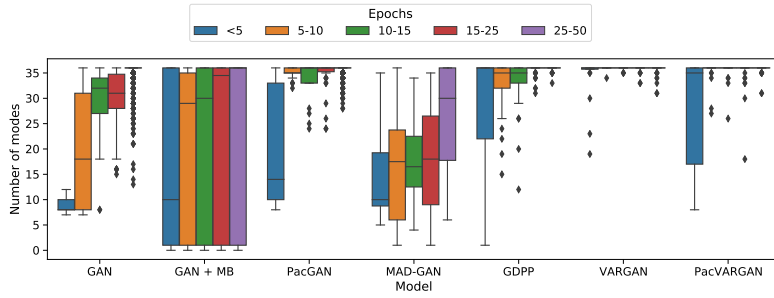
Further analysis over the 50 epoch training process for 2D ring data shows that VARGAN has a quicker convergence process, and leads to a better performance for 2D ring data at the initial epochs compared to the other models. Result for 2D grid data with 36 modes is illustrated in Figure 10 and shows a great performance for the VARGAN in number of generated modes, as well as high quality samples. Although all the models except GAN+MB converge to target number of modes, the variance over the repeats points to a better performance for VARGAN. Note that we repeated this analysis with other two synthetic data variants, which lead to similar observations (see Appendix C for more details). Overall, these results largely confirm the fast convergence of VARGAN on earlier epochs of the training. Furthermore, they point to the methodological/architectural differences between different GAN variants.

Table 2: Performance metrics for synthetic datasets averaged over 5 repeats (all the GANs have FF structure, best performing model is bolded)

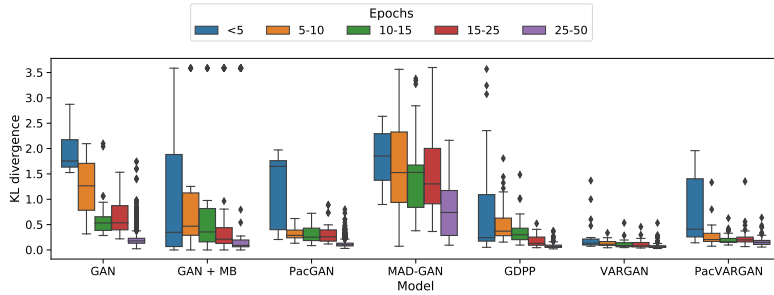
Dataset	Model	Metrics			Time (sec)
		Modes	High quality samples	KL divergence	
Ring 8 modes	GAN	6.20 ± 1.72	0.87 ± 0.03	0.69 ± 0.24	2,731 ± 56
	GAN + MB	4.00 ± 2.60	0.56 ± 0.30	0.80 ± 0.45	693 ± 26
	PacGAN	8.00 ± 0.00	0.71 ± 0.09	0.03 ± 0.02	2,790 ± 6
	MAD-GAN	3.66 ± 2.42	0.25 ± 0.36	1.25 ± 0.57	1,393 ± 73
	GDPP	5.00 ± 1.26	0.60 ± 0.20	1.18 ± 0.21	1,962 ± 182
	VARGAN	4.80 ± 0.40	0.71 ± 0.23	1.05 ± 0.09	1,480 ± 31
Grid 25 modes	PacVARGAN	8.00 ± 0.00	0.32 ± 0.03	0.17 ± 0.07	1,477 ± 16
Grid 25 modes	GAN	25.00 ± 0.00	0.85 ± 0.04	0.45 ± 0.14	3,608 ± 124
	GAN + MB	5.60 ± 9.77	0.76 ± 0.38	1.94 ± 1.55	962 ± 2
	PacGAN	25.00 ± 0.00	0.66 ± 0.07	0.15 ± 0.04	3,642 ± 89
	MAD-GAN	24.80 ± 0.40	0.63 ± 0.23	0.57 ± 0.89	1,679 ± 81
	GDPP	25.00 ± 0.00	0.67 ± 0.02	0.26 ± 0.04	2,463 ± 85
	VARGAN	25.00 ± 0.00	0.80 ± 0.04	0.16 ± 0.06	814 ± 23
Grid 36 modes	PacVARGAN	25.00 ± 0.00	0.59 ± 0.02	0.15 ± 0.05	833 ± 3
Grid 36 modes	GAN	36.00 ± 0.00	0.84 ± 0.06	0.18 ± 0.06	6,154 ± 201
	GAN + MB	21.80 ± 17.39	0.66 ± 0.34	0.75 ± 1.41	1,136 ± 4
	PacGAN	36.00 ± 0.00	0.72 ± 0.03	0.09 ± 0.03	6,183 ± 228
	MAD-GAN	32.00 ± 6.92	0.57 ± 0.28	0.39 ± 0.40	1,804 ± 3
	GDPP	35.80 ± 0.40	0.70 ± 0.02	0.13 ± 0.11	2,712 ± 306
	VARGAN	36.00 ± 0.00	0.73 ± 0.02	0.05 ± 0.01	761 ± 6
Grid 36 modes	PacVARGAN	36.00 ± 0.00	0.66 ± 0.01	0.11 ± 0.04	774 ± 4

4.2.2 Results with stacked MNIST dataset

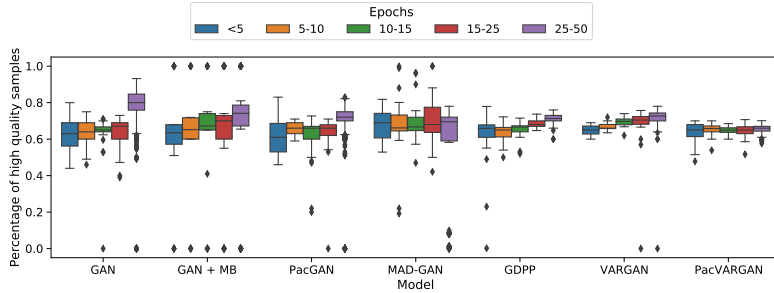
Table 3 summarizes the performance of convolutional (Conv) and feed-forward (FF) structures for different GAN models over stacked MNIST data. The results show that, overall, all the models perform well for both structures. FF (vanilla) GAN captures all the modes, and attains a high inception score and a low KL divergence. GDPP and VARGAN with FF structures also generate a high number of modes and a low KL divergence. Results with convolutional structures show VARGAN as the best performing model with high number of modes, low KL divergence and high inception score. Compared to its FF counterpart, VARGAN performance drops slightly with convolutional structure, however, run time improves significantly. In contrast, PacVARGAN performance benefits significantly from the convolutional structure. The results also confirm that the MB method fails to perform well with FF structure (similar to synthetic data), and its performance improve with convolutional structure. It is worth mentioning that FF



(a) Number of modes



(b) KL divergence



(c) Percentage of high quality samples

Fig. 10: Comparison of different GAN models on synthetic 2D grid data with 36 modes (results are averaged over 5 repeats)

PacGAN model performs slightly worse than its convolutional counterpart. One possible reason for this behaviour might be the PacGAN discriminator structure which combines m samples, and changes the image data input in the FF model case. On other hand, in convolutional models, PACGAN channel factor gets multiplied by m and image structure remains the same.

We note that the number of uniquely generated modes for convolutional PacGAN, and GDPP models matches the results in (Lin et al., 2018; Elfeki et al., 2019) studies. We also examine the models' performance over the training epochs using GANs with convolutional structures (see Appendix C). We find that VAR-

Table 3: Performance metrics for stacked MNIST dataset (with 1000 modes) averaged over 5 repeats (best performing model is bolded)

Structure	Models	Metrics			Time (sec)
		Modes	Inception Score	KL divergence	
FF	GAN	1000 ± 0	1.74 ± 0.01	0.13 ± 0.00	981 ± 0
	GAN + MB	790 ± 257	1.61 ± 0.35	1.10 ± 1.18	1,447 ± 2
	PacGAN	920 ± 10	1.82 ± 0.05	0.79 ± 0.05	1,094 ± 9
	MAD-GAN	994 ± 11	1.56 ± 0.02	0.72 ± 0.12	1,589 ± 30
	GDPP	995 ± 2	1.74 ± 0.04	0.40 ± 0.03	2,467 ± 14
	VARGAN	999 ± 0	1.73 ± 0.02	0.24 ± 0.00	4,686 ± 17
	PacVARGAN	794 ± 42	1.95 ± 0.10	1.19 ± 0.14	4,862 ± 1
Conv	GAN	956 ± 23	1.88 ± 0.06	0.39 ± 0.11	1,203 ± 2
	GAN + MB	916 ± 54	2.09 ± 0.09	0.76 ± 0.19	1,978 ± 0
	PacGAN	935 ± 20	2.09 ± 0.11	0.84 ± 0.13	1,981 ± 1
	MAD-GAN	959 ± 11	1.99 ± 0.05	0.87 ± 0.11	5,532 ± 7
	GDPP	943 ± 52	2.18 ± 0.07	0.69 ± 0.23	3,334 ± 20
	VARGAN	997 ± 1	2.16 ± 0.02	0.34 ± 0.06	2,336 ± 11
	PacVARGAN	996 ± 2	2.14 ± 0.04	0.30 ± 0.03	2,243 ± 3

GAN and PacVARGAN show fast early convergence in terms of all three metrics, which makes them great candidates for artificial data generation. In addition, earlier convergence can be beneficial in terms of speed of GAN training.

4.2.3 Results with EES dataset

Table 4 shows the model performance for feed-forward and convolutional structures over 9×9 and 19×19 EES designs. Overall, results indicate that convolutional models generally have a better performance compared to feed-forward models. For 9×9 designs, for the FF structures, VARGAN, GDPP and GAN create high number of unique modes as well as achieving reasonable accuracy with GDPP achieving the best KL divergence. On the other hand, training time is significantly higher for GDPP compared to GAN and VARGAN. PacGAN performs poorly for FF structures for both 9×9 and 19×19 designs, similar to stacked MNIST. MADGAN with five generators does not perform well for FF structure, and completely collapse and generate one high quality sample with this structure.

In convolutional models, GAN, GAN+MB, VARGAN and PacVARGAN generate the highest number of high pass designs. Lowest KL divergence values are also achieved by GAN+MB. However, the training time for GAN+MB is excessively high, and approximately 10 times higher than VARGAN model for the 9×9 designs.

Intuitively, we expect the performance to deteriorate for the convolutional models in 19×19 designs compared to 9×9 designs. The input in this case is a two

Table 4: Performance metrics for feed-forward and convolutional structures on 9×9 and 19×19 EES designs with 2 categories averaged over 5 repeats (Best performing model is bolded)

Design Structure	Models	Modes		Accuracy		KL divergence	Time (sec)	
		HP	LP	HP	LP			
9×9	FF	GAN	14,572 \pm 94	6,653 \pm 112	0.3121 \pm 0.0150	0.6774 \pm 0.0164	0.00047 \pm 0.00067	677 \pm 9
		GAN + MB	11,654 \pm 5,828	5,071 \pm 2,534	0.4284 \pm 0.2480	0.5707 \pm 0.2505	0.17226 \pm 0.34417	672 \pm 12
		PacGAN	2,603 \pm 757	1,148 \pm 303	0.2970 \pm 0.0181	0.7078 \pm 0.0180	0.00066 \pm 0.00026	663 \pm 1
		MAD-GAN	-	-	-	-	-	-
		GDPP	14,580 \pm 175	6,577 \pm 191	0.3118 \pm 0.0131	0.6862 \pm 0.0132	0.00026 \pm 0.00042	2,969 \pm 19
	Conv	VARGAN	14,793 \pm 137	6,388 \pm 259	0.2945 \pm 0.0128	0.7015 \pm 0.0166	0.00060 \pm 0.00054	996 \pm 13
		PacVARGAN	1,939 \pm 1,070	826 \pm 431	0.2716 \pm 0.0615	0.7264 \pm 0.0497	0.01053 \pm 0.01516	929 \pm 4
		GAN	14,928 \pm 107	6,592 \pm 159	0.1822 \pm 0.0150	0.4035 \pm 0.0177	0.00040 \pm 0.00020	3,704 \pm 1,083
		GAN + MB	15,009 \pm 118	6,716 \pm 95	0.1727 \pm 0.0011	0.3739 \pm 0.0148	0.00010 \pm 0.00008	18,133 \pm 1,805
		PacGAN	14,881 \pm 146	6,714 \pm 210	0.2315 \pm 0.0168	0.4976 \pm 0.0264	0.00062 \pm 0.00029	1,384 \pm 32
19×19	FF	MAD-GAN	359 \pm 469	144 \pm 135	0.0431 \pm 0.0773	0.0301 \pm 0.0496	0.43074 \pm 0.34093	2,414 \pm 20
		GDPP	11,899 \pm 5,892	5,303 \pm 2,602	0.1487 \pm 0.0267	0.2916 \pm 0.1264	0.00292 \pm 0.00579	3,036 \pm 66
		VARGAN	14,962 \pm 164	6,659 \pm 123	0.1608 \pm 0.0218	0.3537 \pm 0.0448	0.00014 \pm 0.00015	1,841 \pm 487
		PacVARGAN	14,829 \pm 224	6,729 \pm 179	0.2131 \pm 0.0065	0.4567 \pm 0.0207	0.00054 \pm 0.00059	3,072 \pm 1,130
		GAN	13,148 \pm 7,349	6,351 \pm 3,135	0.3374 \pm 0.0911	0.6576 \pm 0.0942	0.07343 \pm 0.05317	439 \pm 12
	Conv	GAN + MB	9,698 \pm 5,824	4,443 \pm 2,139	0.3621 \pm 0.1208	0.6260 \pm 0.1191	0.06655 \pm 0.03573	448 \pm 29
		PacGAN	2,232 \pm 1,271	1,078 \pm 741	0.4046 \pm 0.3167	0.5928 \pm 0.3152	0.26998 \pm 0.25194	369 \pm 30
		MAD-GAN	-	-	-	-	-	-
		GDPP	5,232 \pm 5,206	2,625 \pm 1,196	0.4412 \pm 0.2078	0.5669 \pm 0.2069	0.09441 \pm 0.07688	1,241 \pm 38
		VARGAN	13,534 \pm 6,718	5,204 \pm 2,954	0.2784 \pm 0.0917	0.7155 \pm 0.0895	0.11176 \pm 0.06120	673 \pm 52
19×19	FF	PacVARGAN	11,266 \pm 3,077	4,476 \pm 1,696	0.2810 \pm 0.0426	0.7153 \pm 0.0443	0.10882 \pm 0.03999	637 \pm 21
		GAN	237 \pm 229	258 \pm 346	0.6799 \pm 0.2050	0.3216 \pm 0.2050	0.17950 \pm 0.22395	975 \pm 60
		GAN + MB	521 \pm 611	550 \pm 670	0.6138 \pm 0.2615	0.3839 \pm 0.2600	0.20468 \pm 0.25432	3,766 \pm 60
		PacGAN	15,343 \pm 1,180	7,260 \pm 1,714	0.6805 \pm 0.0442	0.3193 \pm 0.0471	0.07148 \pm 0.03324	908 \pm 11
		MAD-GAN	3,166 \pm 2,037	689 \pm 860	0.0275 \pm 0.0477	0.1431 \pm 0.1108	0.26012 \pm 0.08118	2,256 \pm 39
	Conv	GDPP	501 \pm 451	271 \pm 329	0.7499 \pm 0.3189	0.2509 \pm 0.3192	0.42096 \pm 0.24309	1,562 \pm 73
		VARGAN	1,848 \pm 1,316	896 \pm 415	0.6114 \pm 0.2360	0.3878 \pm 0.2379	0.15896 \pm 0.18456	578 \pm 50
		PacVARGAN	13,965 \pm 1,039	5,318 \pm 1,606	0.7399 \pm 0.0672	0.2574 \pm 0.0696	0.13430 \pm 0.08211	467 \pm 50

dimensional matrix with two symmetrical parts, and the model should figure out its symmetry to generate acceptable designs. This creates a more difficult task compared to the feed-forward models and 9×9 design generation. It is important to note that the entire design search space is not available in 19×19 case. We observe that all the models outperform the vanilla GAN with high number of uniquely generated modes. Moreover, PacGAN, VARGAN and PacVARGAN report the lowest KL divergence compared to the rest of the models. Overall, for 19×19 designs, best performance is achieved by PACGAN with convolutional structures, followed up by PacVARGAN. In general, we observe more robustness for the convolutional structures as evidenced by lower standard deviation over a variety of performance metrics. We also find that the convergence of models over

training epochs does not show any significant superiority for VARGAN compared to other GAN models for the EES dataset.

4.3 Impact of conditioning on mode collapse

Mao et al. (2019) argue that conditioning distracts the focus of generator from input noise, which is responsible to create variant designs. As a result, the generator is encouraged to create deterministic outputs based on the conditioned vector, causing mode collapse. To investigate the effect of conditioning on mode collapse, we have selected the best performing models from Section 4.2.3 to experiment with their conditional version. Results for this experiment are reported in Table 5.

Table 5: Comparison of conditioned and unconditioned models on EES designs (bolded models present the best performing model among the conditioned ones)

Design Structure	Models	Condition	Modes		Accuracy		KL divergence
			HP	LP	HP	LP	
9×9	FF	GDPP No	14,580 ± 175	6,577 ± 191	0.3118 ± 0.0131	0.6862 ± 0.0132	0.00026 ± 0.00042
		GDPP Yes	11,441 ± 198	6,146 ± 122	0.9366 ± 0.0072	0.9778 ± 0.0073	0.06611 ± 0.00292
	MSGAN Yes	11,513 ± 252	6,701 ± 200	0.9556 ± 0.0091	0.9820 ± 0.0053	0.07120 ± 0.00339	
	VARGAN No	14,793 ± 137	6,388 ± 259	0.2945 ± 0.0128	0.7015 ± 0.0166	0.00060 ± 0.00054	
	VARGAN Yes	11,338 ± 364	6,083 ± 321	0.9576 ± 0.0062	0.9789 ± 0.0030	0.07266 ± 0.00307	
	Conv	PacGAN No	14,881 ± 146	6,714 ± 210	0.2315 ± 0.0168	0.4976 ± 0.0264	0.00062 ± 0.00029
		PacGAN Yes	11,572 ± 3,856	5,585 ± 1,917	0.5229 ± 0.0361	0.7368 ± 0.0893	0.01101 ± 0.00637
		MSGAN Yes	14,962 ± 135	7,280 ± 72	0.5672 ± 0.0185	0.8410 ± 0.0168	0.00660 ± 0.00225
		VARGAN No	14,962 ± 164	6,659 ± 123	0.1608 ± 0.0218	0.3537 ± 0.0448	0.00014 ± 0.00015
		VARGAN Yes	4,927 ± 6,264	2,217 ± 2,851	0.4067 ± 0.3674	0.4236 ± 0.3543	0.10876 ± 0.13333
PacVARGAN No		14,829 ± 224	6,729 ± 179	0.2131 ± 0.0065	0.4567 ± 0.0207	0.00054 ± 0.00059	
PacVARGAN Yes	9,207 ± 5,348	4,191 ± 2,581	0.4111 ± 0.1828	0.7138 ± 0.1223	0.00792 ± 0.00647		
19×19	FF	GAN No	13,148 ± 7,349	6,351 ± 3,135	0.3374 ± 0.0911	0.6576 ± 0.0942	0.07343 ± 0.05317
		GAN Yes	4,712 ± 6,440	1,356 ± 1,472	0.1264 ± 0.0649	0.8762 ± 0.0641	0.34576 ± 0.17531
		MSGAN Yes	6,634 ± 8,488	3,639 ± 4,469	0.2830 ± 0.1837	0.7371 ± 0.1644	0.20766 ± 0.26400
		VARGAN No	13,534 ± 6,718	5,204 ± 2,954	0.2784 ± 0.0917	0.7155 ± 0.0895	0.11176 ± 0.06120
		VARGAN Yes	7,628 ± 9,566	2,896 ± 3,541	0.1296 ± 0.1506	0.6807 ± 0.3634	0.43210 ± 0.28316
	Conv	PacGAN No	15,343 ± 1,180	7,260 ± 1,714	0.6805 ± 0.0442	0.3193 ± 0.0471	0.07148 ± 0.03324
		PacGAN Yes	13,393 ± 8,004	4,361 ± 2,720	0.6765 ± 0.1081	0.1165 ± 0.0771	0.19064 ± 0.12417
		MSGAN No	2,450 ± 2,747	1,353 ± 1,462	0.7131 ± 0.2232	0.2592 ± 0.2164	0.24830 ± 0.25369
		VARGAN No	1,848 ± 1,316	896 ± 415	0.6114 ± 0.2360	0.3878 ± 0.2379	0.15896 ± 0.18456
		VARGAN Yes	1,775 ± 637	751 ± 407	0.6184 ± 0.1575	0.2080 ± 0.1580	0.12574 ± 0.11315
		PacVARGAN No	13,965 ± 1,039	5,318 ± 1,606	0.7399 ± 0.0672	0.2574 ± 0.0696	0.13430 ± 0.08211
		PacVARGAN Yes	1,126 ± 776	675 ± 561	0.7705 ± 0.2262	0.1176 ± 0.1161	0.32746 ± 0.24215

We observe that, for all the models, conditioning reduces the number of uniquely generated modes over both designs. Mao et al. (2019)’s MSGAN for conditional

GANs outperforms all the conditioned versions of the models, except the PacGAN convolutional version for 19×19 designs. We note that the conditional version of VARGAN for the feed-forward models outperforms the MSGAN in both uniquely generated modes and KL divergence. Moreover, conditional versions of VARGAN and PacVARGAN consistently lead to worse performance compared to their unconditional versions, indicating that there is no need to use a conditioned model to create reasonable number of samples for each category/mode for VARGAN variants.

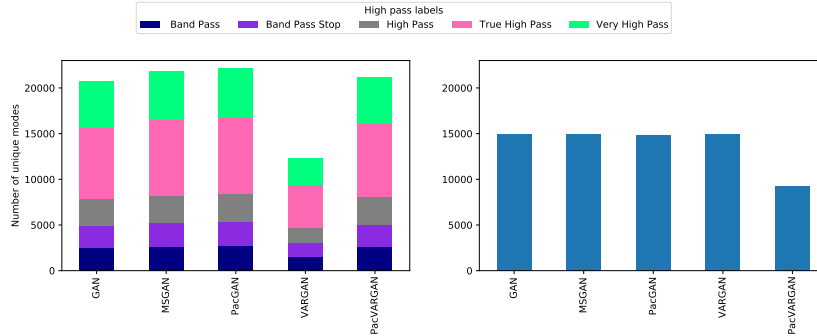
EES data with 8 categories EES designs of size 9×9 can be further categorized to have eight classes (Mohammadjafari et al., 2021). We next compare the effect of increasing the number of conditioned categories on diversity of generated samples. Specifically, we use best performing unconditioned models and condition them on two and eight categories. Table 6 presents the results for convolutional GAN, PacGAN, MSGAN and VARGAN variants for eight categories.

Table 6: Performance metrics reported for 9×9 EES designs using convolutional models for 8 categories averaged over 5 repeats (HP 1: Band Pass, HP 2: Band Pass Stop, HP 3: High Pass, HP 4: True High Pass, HP 5: Very High Pass, LP 1: Band Stop, LP 2: Low Pass, LP 3: Stop Pass)

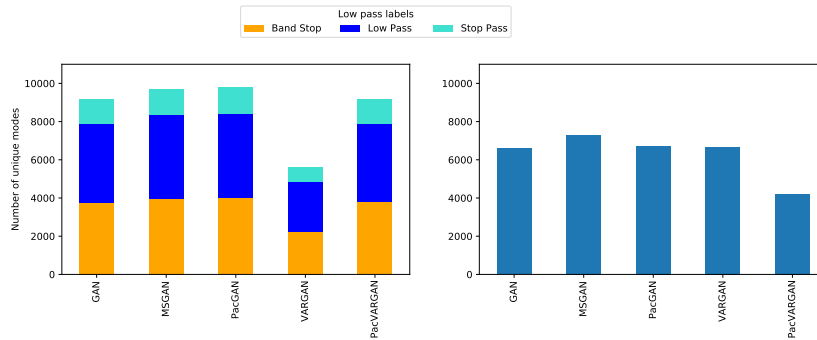
Category	GAN	MSGAN	PacGAN	VARGAN	PacVARGAN	Total samples	
HP	1	$2,521 \pm 238$	$2,664 \pm 35$	$2,740 \pm 15$	$1,543 \pm 1,170$	$2,605 \pm 279$	2,804
	2	$2,410 \pm 116$	$2,531 \pm 20$	$2,566 \pm 12$	$1,452 \pm 1,116$	$2,479 \pm 166$	2,614
	3	$2,945 \pm 169$	$3,035 \pm 45$	$3,130 \pm 14$	$1,730 \pm 1,323$	$2,972 \pm 317$	3,206
	4	$7,819 \pm 446$	$8,322 \pm 27$	$8,359 \pm 25$	$4,702 \pm 3,665$	$8,011 \pm 613$	8,556
	5	$5,093 \pm 311$	$5,344 \pm 28$	$5,399 \pm 23$	$2,933 \pm 2,350$	$5,101 \pm 622$	5,537
	SUM	20,788	21,896	22,194	12,364	21,168	22,717
LP	1	$3,788 \pm 231$	$3,994 \pm 45$	$4,026 \pm 32$	$2,216 \pm 1,758$	$3,816 \pm 373$	4,193
	2	$4,083 \pm 266$	$4,353 \pm 17$	$4,370 \pm 24$	$2,465 \pm 1,959$	$4,090 \pm 537$	4,467
	3	$1,278 \pm 73$	$1,342 \pm 5$	$1,366 \pm 6$	761 ± 581	$1,265 \pm 182$	1,391
	SUM	9,149	9,689	9,762	5,442	9,171	10,051
KL	0.00407 ± 0.00283	0.00337 ± 0.00183	0.00156 ± 0.00100	0.08914 ± 0.10644	0.00394 ± 0.00431		

As expected, PacGAN, MSGAN and PacVARGAN lead to a high performance in this case. Figure 11 provides a comparison of number of unique designs generated for 2 category and 8 category EES datasets. The results show an increase in number of covered modes as the number of conditioned categories increases. The reason behind this result might be the one hot encoding structure of the labels. The large length of labels increases the randomness and diversity of the samples and encourages the generator to avoid creating deterministic results. It is worth

mentioning that VARGAN performance is not dependent on the length of conditions. The variation in samples generated by VARGAN is encouraged by another factor (i.e., MCR values), which removes the limitation to control the length and number of categories.



(a) High pass designs unique modes (right: 8 category data, left: 2 category data)



(b) Low pass designs unique modes (right: 8 category data, left: 2 category data)

Fig. 11: Comparison of total generated unique modes for high pass and low pass designs for 2 and 8 categories over 9×9 designs

5 Conclusions

In this paper, we proposed a new GAN architecture called VARGAN to alleviate the mode collapse issue. VARGAN incorporates a new additional network that measures the samples' diversity. The new network's loss on generated samples is used to penalize the generator and to introduce diversity in the generated samples. We compared the performance of our method with the state-of-the-art GAN architectures on three different datasets. Results show a high performance for the proposed VARGAN architecture, fast convergence and low training times. We also investigated the effect of conditioning on mode collapse in GANs. Our experiments indicate that conditioning reduces the number of generated modes and

induces mode collapse, which can be a cause of deterministic sample generation based on the auxiliary information. We also experimented with MSGAN, which is proposed for reducing mode collapse in conditional GANs. Our results show that, among the conditional models, for feed-forward structures, conditional VARGAN shows slightly better performance compared to MSGAN, whereas, for convolutional structures, MSGAN outperforms conditional VARGAN. Furthermore, we examine the effect of conditioning length on the mode collapse. Our analysis with EES dataset shows that mode collapse happens when generator ignores the noise randomness, and creates deterministic results based on conditions. We observe a resistance of VARGAN to the condition vector length, which points out to the different architecture of VARGAN compared to the existing models.

Our study contributes to a better understanding of methodologies to address mode collapse issue, however, evaluating mode collapse remains a challenging task. In this study, we limit the evaluation of the experiments to the performance metrics discussed in previous studies on mode collapse in GANs. In our analysis, we solely focus on one network architecture extracted from other studies in the literature, which may affect the models' performance. In future research, we plan to design more extensive hyperparameter tuning experiments to check the model's capabilities across different architectures. We also have selected one architecture for our VarNet model inspired by Lin et al. (2018), which can be further improved to better serve the purpose of diversity evaluation. Specifically, we can integrate a computational loss based on the designs' differences to our generator's loss function.

References

- Arjovsky M, Bottou L (2017) Towards principled methods for training generative adversarial networks. arXiv preprint arXiv:170104862
- Arjovsky M, Chintala S, Bottou L (2017) Wasserstein gan. arXiv preprint arXiv:170107875
- Bin H, Weihai C, Xingming W, Chun-Liang L (2017) High-quality face image sr using conditional generative adversarial networks. arXiv preprint arXiv:170700737
- Brock A, Donahue J, Simonyan K (2018) Large scale gan training for high fidelity natural image synthesis. arXiv preprint arXiv:180911096
- Che T, Li Y, Jacob AP, Bengio Y, Li W (2016) Mode regularized generative adversarial networks. arXiv preprint arXiv:161202136
- Elfeki M, Couprie C, Riviere M, Elhoseiny M (2019) Gdpp: Learning diverse generations using determinantal point processes. In: International Conference on Machine Learning, pp 1774–1783
- Ghosh A, Kulharia V, Namboodiri VP, Torr PH, Dokania PK (2018) Multi-agent diverse generative adversarial networks. In: Proceedings of the IEEE conference on computer vision and pattern recognition, pp 8513–8521
- Gulrajani I, Ahmed F, Arjovsky M, Dumoulin V, Courville AC (2017) Improved training of wasserstein gans. In: Advances in neural information processing systems, pp 5767–5777
- Gurumurthy S, Kiran Sarvadevabhatla R, Venkatesh Babu R (2017) Deligan: Generative adversarial networks for diverse and limited data. In: Proceedings of the IEEE conference on computer vision and pattern recognition, pp 166–174

- Hoang Q, Nguyen TD, Le T, Phung D (2018) Mgan: Training generative adversarial nets with multiple generators. In: International conference on learning representations
- Isola P, Zhu JY, Zhou T, Efros AA (2017) Image-to-image translation with conditional adversarial networks. In: Proceedings of the IEEE conference on computer vision and pattern recognition, pp 1125–1134
- Karras T, Aila T, Laine S, Lehtinen J (2017) Progressive growing of gans for improved quality, stability, and variation. arXiv preprint arXiv:171010196
- Ledig C, Theis L, Huszár F, Caballero J, Cunningham A, Acosta A, Aitken A, Tejani A, Totz J, Wang Z, et al. (2017) Photo-realistic single image super-resolution using a generative adversarial network. In: Proceedings of the IEEE conference on computer vision and pattern recognition, pp 4681–4690
- Li W, Xu L, Liang Z, Wang S, Cao J, Lam TC, Cui X (2021) Jdgan: Enhancing generator on extremely limited data via joint distribution. *Neurocomputing* 431:148–162
- Lin Z, Khetan A, Fanti G, Oh S (2018) Pacgan: The power of two samples in generative adversarial networks. In: Advances in neural information processing systems, pp 1498–1507
- Mao Q, Lee HY, Tseng HY, Ma S, Yang MH (2019) Mode seeking generative adversarial networks for diverse image synthesis. In: Proceedings of the IEEE/CVF Conference on Computer Vision and Pattern Recognition, pp 1429–1437
- Metz L, Poole B, Pfau D, Sohl-Dickstein J (2016) Unrolled generative adversarial networks. CoRR abs/1611.02163, URL <http://arxiv.org/abs/1611.02163>, 1611.02163
- Mirza M, Osindero S (2014) Conditional generative adversarial nets. arXiv preprint arXiv:14111784
- Mohammadjafari S, Ozyegen O, Cevik M, Kavurmacioglu E, Ethier J, Basar A (2021) Designing mm-wave electromagnetic engineered surfaces using generative adversarial networks. *Neural Computing and Applications* pp 1–15
- Mok TC, Chung AC (2018) Learning data augmentation for brain tumor segmentation with coarse-to-fine generative adversarial networks. In: International MICCAI Brainlesion Workshop, Springer, pp 70–80
- Park DK, Yoo S, Bahng H, Choo J, Park N (2018) Megan: Mixture of experts of generative adversarial networks for multimodal image generation. arXiv preprint arXiv:180502481
- Radford A, Metz L, Chintala S (2015) Unsupervised representation learning with deep convolutional generative adversarial networks. arXiv preprint arXiv:151106434
- Salimans T, Goodfellow I, Zaremba W, Cheung V, Radford A, Chen X (2016) Improved techniques for training gans. In: Advances in neural information processing systems, pp 2234–2242
- Srivastava A, Valkov L, Russell C, Gutmann MU, Sutton C (2017) Veegan: Reducing mode collapse in gans using implicit variational learning. In: Advances in Neural Information Processing Systems, pp 3308–3318
- Tolstikhin IO, Gelly S, Bousquet O, Simon-Gabriel CJ, Schölkopf B (2017) Adagan: Boosting generative models. In: Advances in Neural Information Processing Systems, pp 5424–5433
- Zhong P, Mo Y, Xiao C, Chen P, Zheng C (2019) Rethinking generative mode coverage: A pointwise guaranteed approach. arXiv preprint arXiv:190204697

- Zhu JY, Park T, Isola P, Efros AA (2017a) Unpaired image-to-image translation using cycle-consistent adversarial networks. In: Proceedings of the IEEE international conference on computer vision, pp 2223–2232
- Zhu JY, Zhang R, Pathak D, Darrell T, Efros AA, Wang O, Shechtman E (2017b) Multimodal image-to-image translation by enforcing bi-cycle consistency. In: Advances in neural information processing systems, pp 465–476
- Zuo Z, Zhao L, Zhang H, Mo Q, Chen H, Wang Z, Li A, Qiu L, Xing W, Lu D (2019) Ldmgan: Reducing mode collapse in gans with latent distribution matching

A Selection of MCR formulation and its parameters

We have explored three different formulations for the MCR values. Equation (5) presents a linear relationship between MCR value and percentage of covered modes.

$$MCR = \begin{cases} \frac{n}{N} & n = 2, \dots, N-1, n \mid B \\ 0 & n = 1 \end{cases} \quad (5)$$

Equation (6) models a relationship that achieves early convergence to reward the model with low generator error.

$$MCR = \begin{cases} \frac{L}{1+S_1 \cdot e^{-\frac{n}{N} \cdot S_2}} & n = 2, \dots, N-1, n \mid B \\ 0 & n = 1 \end{cases} \quad (6)$$

Equation (7) models a relationship where it avoids rewarding the generator too early to keep it motivated.

$$MCR = \begin{cases} \frac{L}{1+S_1 \cdot e^{-\frac{n-N}{N} \cdot S_2}} & n = 2, \dots, N-1, n \mid B \\ 0 & n = 1 \end{cases} \quad (7)$$

Figure 12 shows the trajectory of different formulations based on the percentage of covered modes. Firstly, we have experimented with constant values of L , S_1 and S_2 for different for-

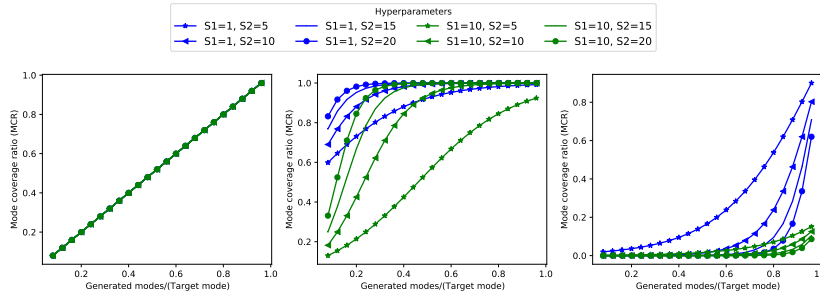


Fig. 12: MCR value based on number of generated modes divided by target modes for different equations. Left, middle and right figures in order present Equation (5), (6) and (7).

mutations on synthetic data with 36 modes. Our results illustrated in Figure 13 indicate that Equation (6) is presenting a suitable trajectory for MCR values over the percentage of covered modes.

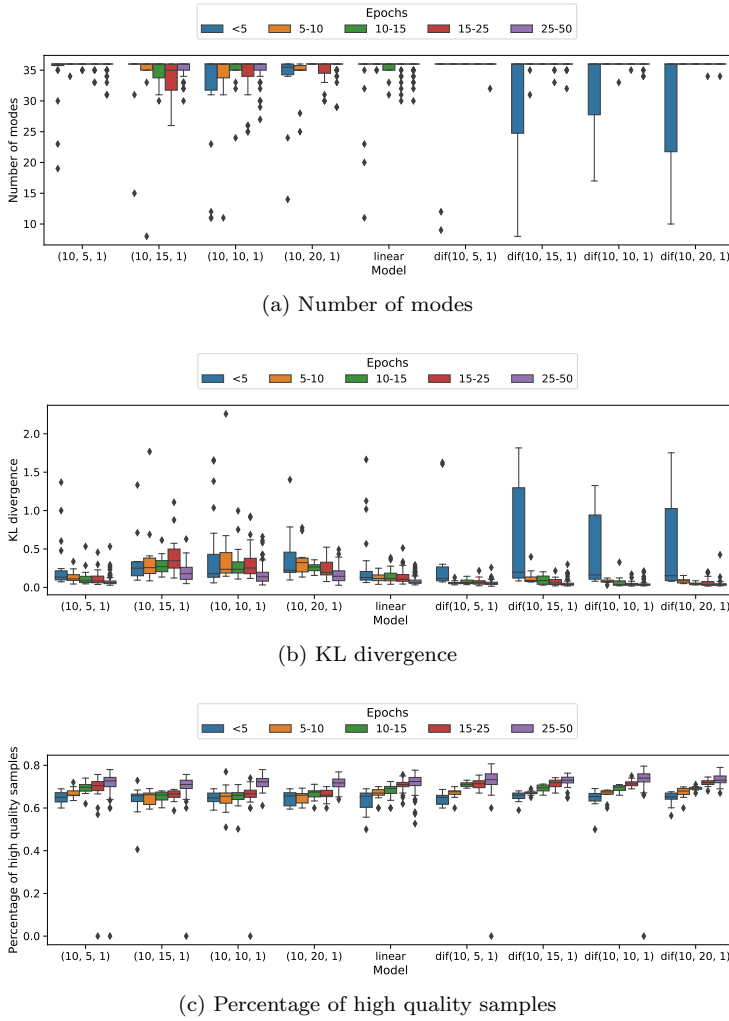
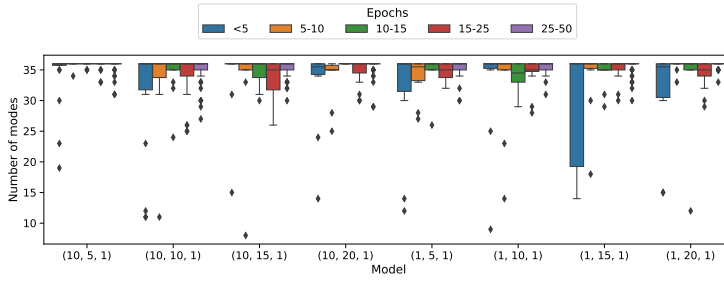


Fig. 13: Comparison of different MCR formulations on synthetic 2D grid data with 36 modes averaged over 5 repeats

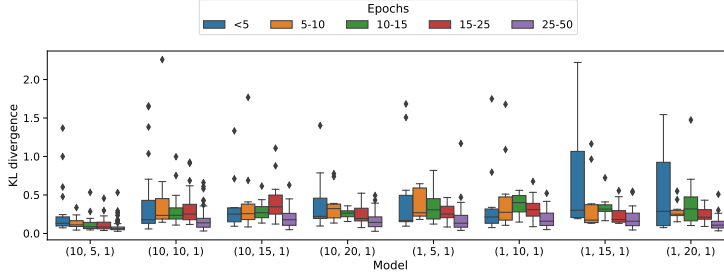
Finally, we have used different values of L , S_1 and S_2 on synthetic data with 36 modes. The hyperparameter optimization results are illustrated in Figure 14. Equation (6) with L , S_1 and S_2 of 1, 10 and 5 shows an early convergence for all the metrics compared to other formulations and hyperparameters. As shown in Figure 12, L , S_1 and S_2 of 1, 10 and 5 enforce a low initial MCR value with moderate speed of convergence to MCR value of one. In other words, VARGAN performance does not improve by defining a large MCR value for initial low mode coverage or a fast convergence trajectory.

B Architecture of models

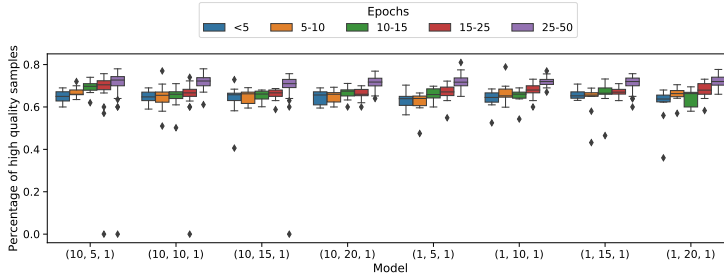
In this section, a detailed summary of GAN architectures is presented. Table 7 presents the feed-forward model architecture used for all the datasets. Table 8 shows the convolutional



(a) Number of modes



(b) KL divergence



(c) Percentage of high quality samples

Fig. 14: Comparison of different hyperparameters for Equation (6) on synthetic 2D grid data with 36 modes averaged over 5 repeats

model architecture used for stacked MNIST dataset. We have modified the architecture for other GAN variants to implement the specific details of their methodology. Convolutional model architecture used for EES dataset is reported in Table 9. Number of convolutional layers is changed to implement both 9×9 and 19×19 designs.

C Detailed results

In this section, performance comparison of GAN models over the epochs is presented. Figure 15 and 16 illustrate the convergence of the models for synthetic data with 8 and 25 modes based on different performance metrics and over epochs. VARGAN and GDPP models seem to have early convergence in the beginning epochs for synthetic data with 8 modes. VARGAN shows

Table 7: Structure of FF GAN model

Network	Number of units	Activation function	Regularization
Generator	512	LeakyReLU	-
	1,024	LeakyReLU	-
	2,048	LeakyReLU	-
	4,096	LeakyReLU	-
	Output size	Sigmoid	-
Discriminator	2,048	LeakyReLU	-
	1,024	LeakyReLU	Dropout(0.3)
	512	LeakyReLU	Dropout(0.3)
	1	Sigmoid	-

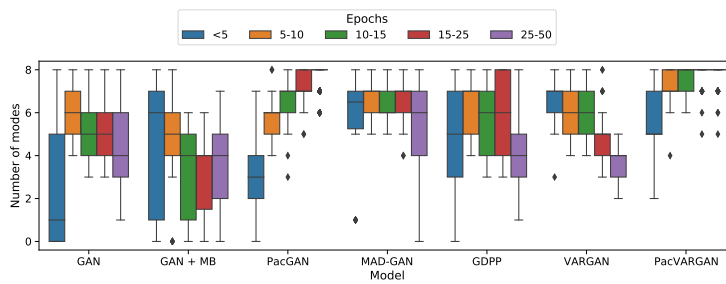
Table 8: Structure of convolutional GAN model for stacked MNIST dataset

Network	Layer	# of channels	Kernel size	Activation function
Generator	Linear	-	-	ReLU
	Conv	256	4	ReLU
	Conv	128	4	ReLU
	Conv	64	4	ReLU
	Conv	3	4	Tanh
Discriminator	Conv	64	4	LeakyReLU
	Conv	128	4	LeakyReLU
	Conv	256	4	LeakyReLU
	Conv	512	4	LeakyReLU
	Linear	-	-	Sigmoid

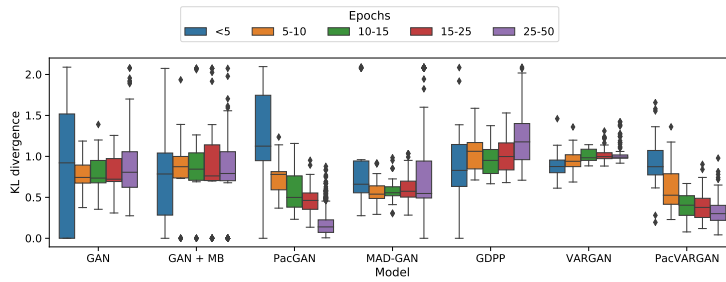
Table 9: Structure of convolutional GAN model for EES dataset

Network	Layer	# of channels	Kernel size	Activation function
Generator	Linear	-	-	LeakyReLU
	Conv	256	3	LeakyReLU
	Con	128	3	LeakyReLU
	Conv	1	3	Sigmoid
Discriminator	Conv	64	3	LeakyReLU
	Conv	128	3	LeakyReLU
	Conv	256	3	LeakyReLU
	Linear	-	-	Sigmoid

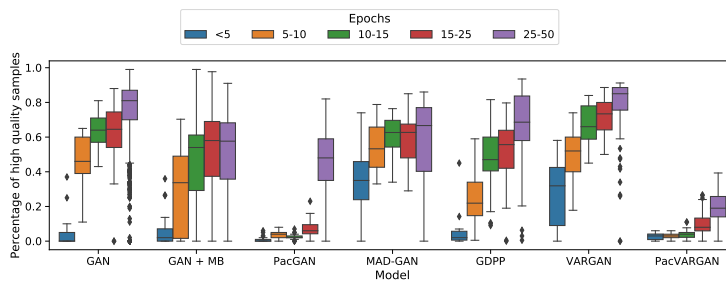
great early convergence on synthetic data with 25 modes as well, and the rest of the models follow it by a large gap.



(a) Number of modes



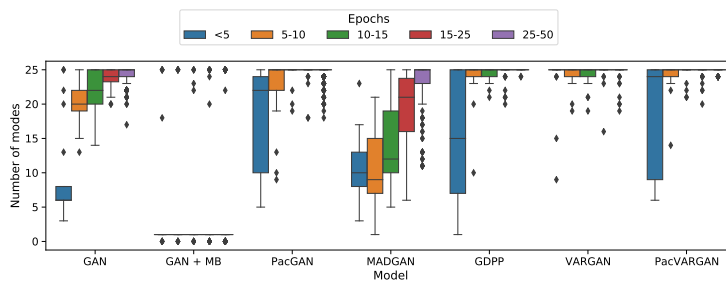
(b) KL divergence



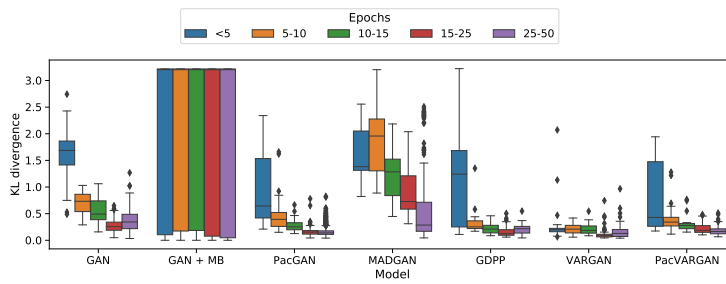
(c) Percentage of high quality samples

Fig. 15: Comparison of different GAN models on synthetic 2D ring data with 8 modes averaged over 5 repeats

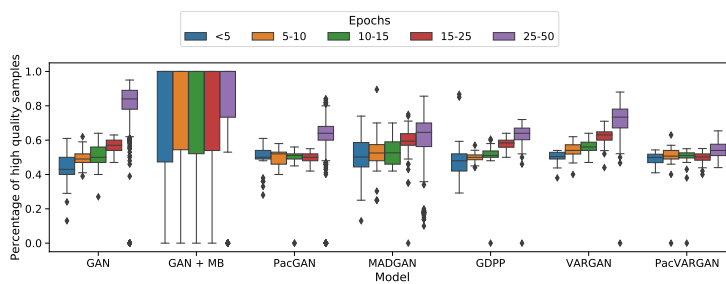
Figure 17 presents the convergence of performance metrics for convolutional GAN models on stacked MNIST data. Both VARGAN and PacVARGAN show great early convergence on all metrics.



(a) Number of modes

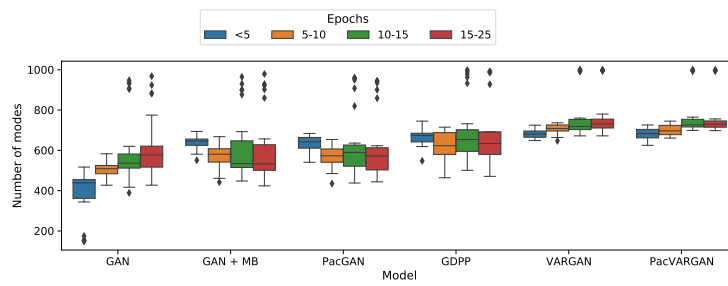


(b) KL divergence

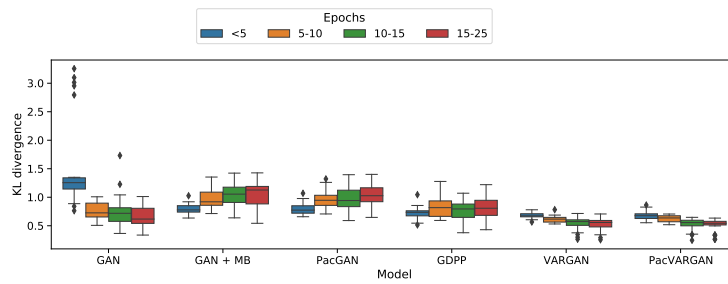


(c) Percentage of high quality samples

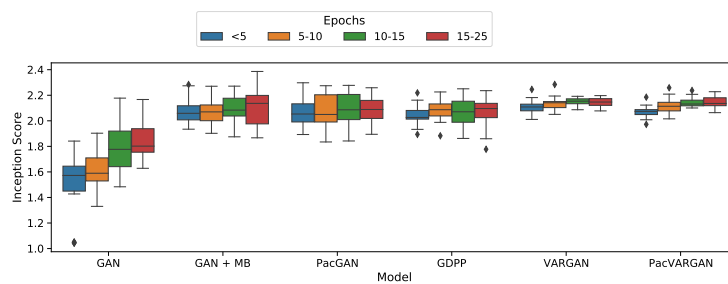
Fig. 16: Comparison of different GAN models on synthetic 2D grid data with 25 modes averaged over 5 repeats



(a) Number of modes



(b) KL divergence



(c) Inception Score

Fig. 17: Performance comparison of different GAN models with convolutional GAN structure for stacked MNIST dataset averaged over 5 repeats